The Onset of Collective Behavior in Social Amoebae

Thomas Gregor,[1]* Koichi Fujimoto,[2]† Noritaka Masaki,[2] Satoshi Sawai[1,2]‡

In the social amoebae *Dictyostelium discoideum*, periodic synthesis and release of extracellular cyclic adenosine 3′,5′-monophosphate (cAMP) guide cell aggregation and commitment to form fruiting bodies. It is unclear whether these oscillations are an intrinsic property of individual cells or if they exist only as a population-level phenomenon. Here, we showed by live-cell imaging of intact cell populations that pulses originate from a discrete location despite constant exchange of cells to and from the region. In a perfusion chamber, both isolated single cells and cell populations switched from quiescence to rhythmic activity depending on the concentration of extracellular cAMP. A quantitative analysis showed that stochastic pulsing of individual cells below the threshold concentration of extracellular cAMP plays a critical role in the onset of collective behavior.

Populations of microorganisms often undergo transitions to coordinated activities depending on nutrient availability and presence of other microbes in the environment. In a process termed "quorum sensing" (*1*), small signaling molecules are synthesized and secreted into the extracellular space. When the concentration of the molecules reaches a threshold, the cell population undergoes a transition to a state that collectively can cope with the new environment. Studies on chemical oscillators (*2*), glycolytic oscillations in yeast (*3*), and a synthetic gene circuit in bacteria (*4*) have demonstrated that synchronized oscillations may rely on a similar quorum sensing–type transition. Unlike in cases where synchronized oscillations appear by entrainment of phase and frequencies of autonomously oscillating elements [e.g., fireflies (*5*), circadian rhythms (*6*), somite segmentation (*7*), Josephson junction arrays (*8*), chemical reactions (*9*), etc. (*10*)], the quorum sensing–type transition is accompanied by a spontaneous change from quiescence to oscillations at the individual level. The transition, referred to as "dynamical quorum sensing," encodes cell-density information in the frequency of the oscillations (*2*, *3*), because the small-molecule threshold may be reached more quickly at higher cell densities. Although the scheme can provide a robust means for a single cell to change its state qualitatively depending on the cell density, exposing the basis of the oscillatory transition in cell populations has remained a challenge (*11*, *12*) because of difficulties in analyzing the dynamics of individual cells and the

[1]Graduate School of Arts and Sciences, University of Tokyo, Tokyo 153-8902, Japan. [2]Exploratory Research for Advanced Technology (ERATO) Complex Systems Biology Project, Japan Science and Technology Agency (JST), Tokyo 153-8902, Japan.

*Present address: Department of Physics, Princeton University, Princeton, NJ 08544, USA.

†Present address: Department of Biological Sciences, Osaka University, Toyonaka 560-0043, Japan.

‡To whom correspondence should be addressed. E-mail: cssawai@mail.ecc.u-tokyo.ac.jp

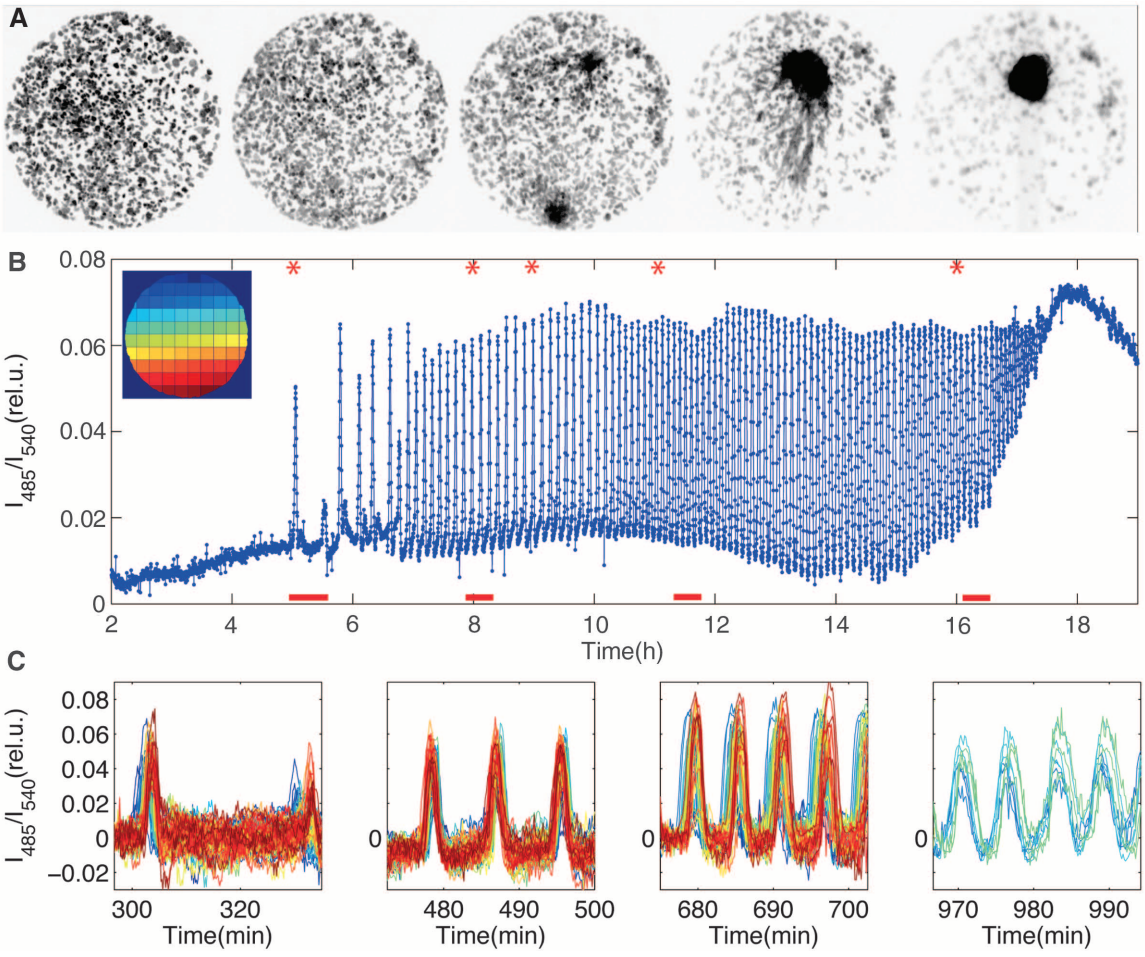

Fig. 1. Live-cell imaging of cAMP signaling during early development of *D. discoideum* cells. (**A**) About 180 cells were confined to a 420-μm-diameter area on hydrophobic agar (*22*). Snapshots were taken at times indicated by the red asterisks in (B). Dark area in rightmost snapshot corresponds to final aggregation site of the population. (**B**) Time course of changes in FRET efficiency, averaged over all cells (time indicates hours after starvation). The fluorescent intensities of the cyan fluorescent protein channel divided by that of the yellow fluorescent protein channel are plotted on the *y* axis. The upper left inset is a colored schematic for the subregions analyzed in (C). (**C**) Enlargements of the time series for each subregion, containing zero to five cells. Red bars indicate time windows in (B), chronologically ordered from left to right. Colors correspond to the colors of the spatial regions displayed in the inset in (B). Small differences in the rising phase of the pulses for individual regions correspond to cAMP waves that are propagating in space (see also fig. S7).

population simultaneously. Moreover, how microorganisms use cellular oscillatory mechanisms to implement complex life-cycle strategies at the population scale remains unexplored.

Chemoattractant signaling in the social amoebae *Dictyostelium discoideum* is one of the best-known examples of cell-cell signaling that mediates cooperation in microorganisms (*13*). When stimulated with extracellular cyclic adenosine 3′,5′-monophosphate (cAMP), cells respond by synthesizing and secreting more cAMP, which results in nondissipating waves of cAMP (*14*, *15*)

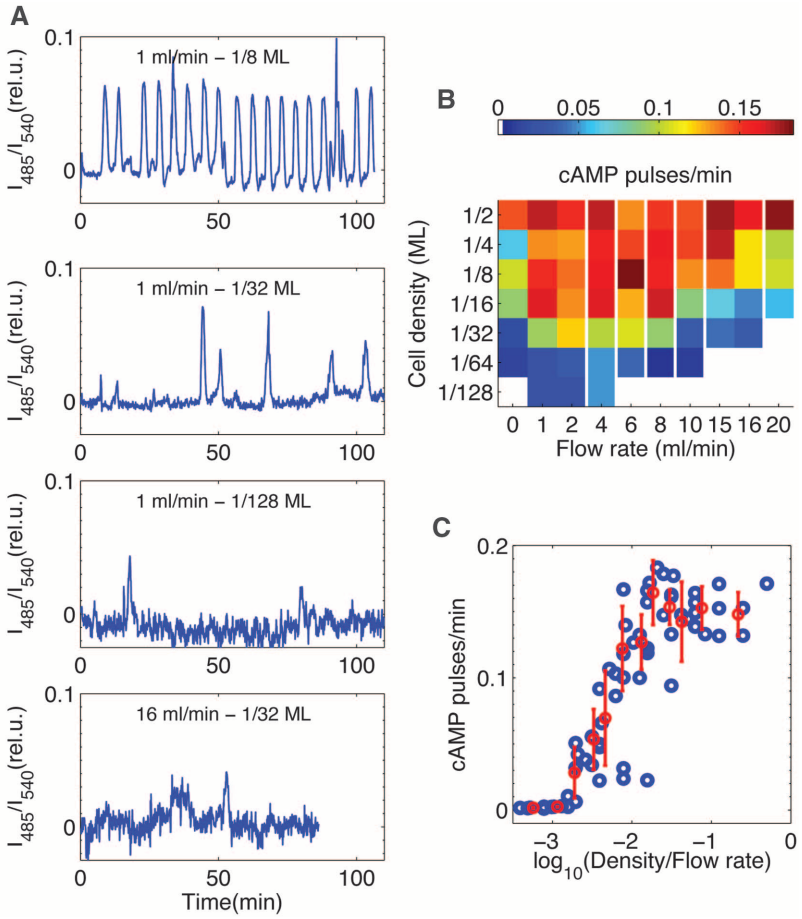

Fig. 2. Synchronized population-level oscillations of cytosolic cAMP. Cells were placed in a perfusion chamber (volume of ~0.25 ml) 4 to 6 hours after starvation. (**A**) Population-averaged behavior at cell densities of 1/8 monolayer (ML; 1 ML unit is 6600 cells/mm^2), 1/32 ML, and 1/64 ML (top to bottom, respectively) under buffer at a fixed flow rate of 1 ml/min. The lowest panel is at 1/32 ML and 16 ml/min. (**B**) A phase diagram summarizes 148 experiments at various densities and flow rates. The mean firing rate (min^{-1}) is represented in color. Red regions display the highest firing rates (period of ~6 min). Sporadic firing occurs in the blue regions (see also fig. S5). White regions correspond to regimes of no spontaneous firing; white vertical lines indicate nonlinear breaks in the *x* axis. (**C**) Firing rate as a function of the ratio between cell density and flow rate (ρ/k) (blue circles). Mean ± SE (indicated in red) are computed from equi-populated bins. Four points around a value of −2 on the *x* axis were considered outliers because they were sampled at very low *k* (flow rates < 1 ml/min), where the effect of extracellular PDE is nonnegligible (*30*).

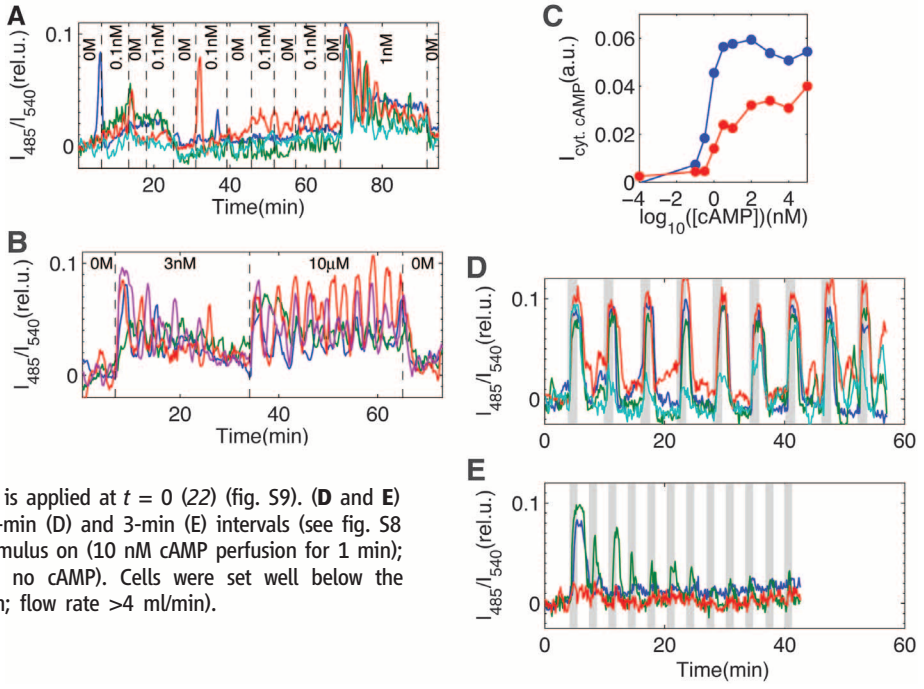

Fig. 3. The cAMP-induced cytosolic cAMP signaling response of isolated individual cells in a perfusion chamber. (**A**) Representative time courses of subthreshold response (four cells are represented by different colors). The concentration of extracellular cAMP was changed at time points indicated by dashed lines (0 M, perfusion with buffer only, no cAMP). (**B**) Damped and persistent oscillations of cytosolic cAMP when perfused with 3 nM and 10 μM exogenous cAMP, respectively (colors indicate four individual cells). (**C**) Single-cell input/output relation of time- and cell-averaged responses to applied cAMP ranging from 100 pM to 100 μM (blue and red lines correspond to 3- and 30-min averages, respectively). The relative cAMP output of an isolated cell for a given input stimulus over a time period *T* is evaluated here by computing the time-integral of I_{485}/I_{540} given by $I_{cyt.cAMP}(T) = \frac{1}{T}\int_0^T I_{485}(t)/I_{540}(t)dt$, where the stimulus is applied at $t = 0$ (*22*) (fig. S9). (**D** and **E**) Individual cells responding to repetitive stimuli at 6-min (D) and 3-min (E) intervals (see fig. S8 for 4-min and 15-min intervals). Shaded regions, stimulus on (10 nM cAMP perfusion for 1 min); white regions, stimulus off (buffer perfusion only, no cAMP). Cells were set well below the transition point shown in Fig. 2C (separation >1mm; flow rate >4 ml/min).

that guides aggregation of individual amoeboid cells. Most of our understanding of the cAMP oscillations in *Dictyostelium* is based on population-level optical-density observations (*15*–*17*) or isotope dilution assays of cAMP on fixed samples (*14*, *18*–*20*). Because such measurements hide possible cell-cell heterogeneities, it is unknown whether the initiation of the periodic behavior is due to synchronization of cells that can autonomously oscillate regardless of interactions with other cells, or whether it is a "dynamical quorum sensing"–type phenomenon (*3*)—i.e., individual cells remain nonoscillatory unless the entire population becomes oscillatory.

To elucidate the onset of the cAMP oscillations, we used a fluorescence resonance energy transfer (FRET)–based sensor (*21*) to directly monitor cytosolic cAMP in live *Dictyostelium* cells (*22*) (fig. S3). Inhibiting synthesis of cAMP inhibited oscillations, confirming that changes in FRET efficiency reflect changes in cytosolic cAMP concentrations (*22*) (fig. S1). A representative time course of development is shown in Fig. 1, A and B (movie S1). Cells began to fire synchronously 5 hours after nutrient deprivation with pulses occurring sporadically every 15 to 30 min (Fig. 1B; 5 to 7 hours). Over the next 2 hours, the period of firing shortened to 8 min and thereafter to 6 min when cells began to aggregate. The entire population participated in the firing from the first pulse (Fig. 1C, leftmost panel). Differences in the phase of the oscillations depending on the regions indicate that pulses propagated in space as waves (fig. S7). Different spatial locations competed for wave initiation (Fig. 1C, second panel from the left). However, a single region eventually dominated and determined the aggregation center (Fig. 1A, middle panel). Tracking of individual cells revealed a continuous exchange of cells to and from the signaling centers. Together, these observations suggest that the oscillations do not originate from autonomous activities of specialized cells, but rather that they probably result from inhomogeneous fluctuations in the concentration of extracellular signaling molecules that favor pulse generation.

To probe the extracellular conditions necessary to initiate periodic pulses, we placed cells in a perfusion chamber that provides rapid mixing and exchange of extracellular buffer to ensure a uniform and controlled environment. Pulsing rates were systematically measured for a wide range of cell densities and dilution rates. Representative data are shown in Fig. 2A. At sufficiently high densities (~10^3 cells/mm^2) and under moderate flow speed (~1 ml/min), cells periodically fire approximately once every 6 min on average (Fig. 2A, top panel), which is typically observed in an intact population near a monolayer density (*14*, *16*, *17*) (Fig. 1B). With decreasing cell density, the synchronized pulses become sporadic and finally cease (Fig. 2A). The dependence of the firing rate on cell density and dilution rate is presented as a phase diagram (Fig. 2B). The frequency of pulsing at flow rates >1 ml/min is proportional to a single parameter, ρ/k, which defines the ratio of cell density ρ to flow rate k (Fig. 2C). The pulsing rate is close to zero when ρ/k is small. As ρ/k is increased, the frequency increases logarithmically and levels off at ~6-min oscillations.

To understand the origin of this dynamical transition, we quantified the response of single isolated cells to continuous application of exogenous cAMP (Fig. 3, A and B). In the absence of extracellular cAMP, cytosolic cAMP concentrations remain steady with some fluctuations (fig. S4). At subnanomolar stimulation, cells pulse randomly (Fig. 3A). Upon application of nanomolar concentrations of cAMP, cells display excitatory behavior (1 nM in Fig. 3A and 3 nM in Fig. 3B)—a sharp transient rise that peaks after ~30 s is followed by smaller peaks that gradually attenuate. Damping of the response becomes less marked at micromolar concentrations of cAMP (Fig. 3B; 10 μM). The oscillatory responses persist at 2.5- to 8-min periods, which vary from cell to cell. The peaks appear even at 100 μM cAMP (fig. S9), well above the saturation dose of the cAMP receptors (*23*), suggesting that cytosolic oscillations can occur without periodic changes in the concentration of extracellular cAMP. However, this persistent oscillatory behavior depends strictly on the presence of extracellular cAMP, because when the stimulus is removed, cytosolic cAMP returns to its prestimulus level within 30 to 60 s (Fig. 3A at 90 min; Fig. 3B at 65 min). From fluorometric measurements, we estimate that the basal and the peak concentrations of cytosolic cAMP correspond on average to ~400 nM and ~10 μM, respectively (fig. S3). Figure 3C summarizes the cytosolic cAMP responses in the form of an input/output relation (see also fig. S9). The input corresponds to the applied cAMP concentrations and the output to the integrated response over two time intervals: (i) 3 min, corresponding to the initial peak of the response (Fig. 3C; blue curve); and (ii) 30 min (red curve). The 3-min interval exhibits a half-maximal output at 0.5 ± 0.1 nM cAMP, suggesting that a cell can be excited by a very low number of cAMP molecules. For the longer interval, the half-maximal concentration is 1.7 ± 0.2 nM owing to damping of the response.

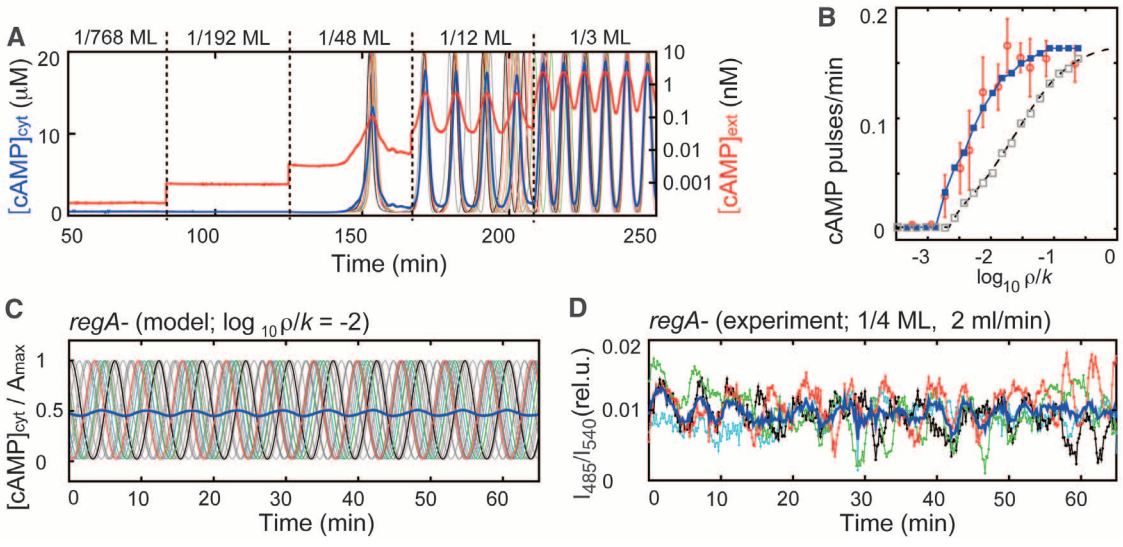

Fig. 4. Dynamical quorum sensing–type transition in a population of excitable/oscillatory switch elements. (**A**) Representative simulated time courses of average cAMP concentrations (cytosolic $[cAMP]_{cyt}$ and extracellular $[cAMP]_{ext}$ in linear and logarithmic scales, respectively). Thin colored lines indicate $[cAMP]_{cyt}$ in individual cells. Cell densities were increased in incremental steps of 1/768 ML, 1/192 ML, 1/48 ML, 1/12 ML, and 1/3 ML at k = 5 ml/min. (**B**) Firing rate as a function of ρ/k as predicted by the coupled phase model with (blue line; eq. S5) or without (gray squares; eq. S5) incorporation of stochastic pulsing. For comparison, see experimental data from Fig. 2C (red circles) and mean-field approximation (dashed black line; eq. S6). (**C**) Model prediction of desynchronization at elevated cytosolic cAMP concentrations [a 10-fold increase in maximum (A_{max}) and basal (A_{bas}) cytosolic cAMP concentrations; eq. S1]. $[cAMP]_{cyt}$ normalized by A_{max} in individual cells (thin gray lines; four cells are highlighted by colors). Blue line indicates population average. (**D**) Poorly synchronized population-level oscillations in *regA*$^-$ mutants whose degradation of intracellular cAMP is reduced (1/4 ML; 2 ml/min). Colors indicate average signals by cells in four 100 μm by 100 μm regions separated by ~150 μm. Blue line indicates average of the four regions.

The results in Figs. 2 and 3 indicate that accumulation of extracellular cAMP ($[cAMP]_{ext}$) in the population is essential for excitatory and oscillatory cell responses. At low ρ/k, if cells secrete cAMP on average at a constant rate r, then $[cAMP]_{ext}$ changes according to

$$\frac{d[cAMP]_{ext}}{dt} = \rho r - \frac{k}{V_T}[cAMP] \quad (1)$$

which states that variations in cell density ρ alter the effective synthesis rate of extracellular cAMP, while the rate of dilution k divided by the chamber volume V_T determines how fast extracellular cAMP is removed. Assuming that the system is at steady state in this regime, $[cAMP]_{ext}$ must be proportional to the parameter ρ/k (eq. S4), and hence Eq. 1 assumes a constant cell secretion rate for cAMP. Isolated cells exposed to extracellular cAMP below the threshold concentration of ~500 pM (Fig. 3C), however, display nonnegligible excitable dynamics that appear to be stochastic (Fig. 3A and fig. S4). This observation matches well with the sporadic pulses observed experimentally at the population level (fig. S5), when ρ/k is near the transition point (i.e., $\rho/k \sim 10^{-3}$ in Fig. 2C). Incorporating first-order secretion (*24*) into Eq. 1, we computed the effective synthesis rate per monolayer cell density to be r = 5.2 nM/min (by eqs. S3 and S8), implying that near the transition point, cells should only be able to accumulate extracellular cAMP of less than ~10 pM (eq. S7). Such low concentrations, however, are more than an order of magnitude below the responsive range of a single cell (Fig. 3C), indicating a limitation of the static picture provided by Eq. 1.

At high ρ/k, the firing rate reaches a plateau (~1/6 min^{-1} in Fig. 2C), which cannot be deduced from the observed cell responses to persistent stimuli (Fig. 3C) alone. When isolated cells are repetitively stimulated with 10 nM cAMP at 6-min intervals, cells responded in pace with the stimuli (Fig. 3D). However, at shorter intervals the response gradually diminished (Fig. 3E and fig. S8A), and at longer intervals random bursts appeared spontaneously (fig. S8B). Thus, an individual *Dictyostelium* cell behaves as a resonance filter that selects a stimulus at 6-min intervals. That is, extracellular cAMP must be removed for a certain time period for cells to respond to further stimuli. Such a time scale is a single-cell–level property. The requirement of cAMP removal is consistent with population experiments that we performed in the absence of flow (<1 ml/min; Fig. 2B). They demonstrate that synchronized oscillations require removal of extracellular cAMP by extracellular phosphodiesterase (PDE, the enzyme that degrades extracellular cAMP) (figs. S2 and S10A). Together with the observed cytosolic oscillations in cells under prolonged stimulation (Fig. 3B), these observations indicate that in addition to the time it takes for the extracellular cAMP to return to its original prepulse concentration (a global process mediated by extracellular PDE), there exist local mechanisms that monitor time intracellularly before individual cells fully recover their state of excitability.

To determine quantitatively the origin of synchronized pulses in the population, we incorporated the observed response behavior into Eq. 1. To this end, the single-cell–level dynamics of cytosolic cAMP is described by a phase equation (eqs. S1 and S2 and fig. S6A) that reproduces the pulsatile cAMP output observed in Fig. 3 (fig. S6B). When such cellular elements are coupled (eq. S5), the population switches from a quiescent to an oscillatory state at a critical cell density (Fig. 4A). The model can accurately reproduce the frequencies of the synchronized oscillations (Fig. 4B; blue line and red circles) only when the random pulsing observed at subnanomolar concentrations (Fig. 3A and fig. S4) is taken into account. Without random pulsing, the curve appears slanted and shifts toward higher ρ/k (Fig. 4B; gray line). Hence, our model confirms the importance of sporadic random firing at the onset of synchronized pulses in the population, as observed experimentally in fig. S5. At subnanomolar concentrations of extracellular cAMP, the probability that a cell is randomly excited increases (Fig. 3A and fig. S4), enhancing the chance for other cells to fire (fig. S6C). A chain reaction of excitation is thus generated that can give rise to synchronized pulses [Fig. 4A (1/48 ML) and fig. S6C] even at subnanomolar concentrations below the threshold. Thus, the question of whether specialized cells initiate synchronized pulses is ill posed; the initiation process is inherently collective and stochastic.

Synthesis of intracellular cAMP requires a receptor-mediated activation of adenylyl cyclase ACA (fig. S1, D to G)—the main enzyme responsible for converting adenosine 5′-triphosphate (ATP) to cAMP during this stage of *Dictyostelium* development. Binding of cAMP to the membrane-bound receptor induces production of phosphatidylinositol 3,4,5-trisphosphate (PIP_3) that recruits an activating factor containing a specific PIP_3-binding domain [pleckstrin homology (PH) domain] to the plasma membrane (*25*). Given the small number of extracellular cAMP molecules necessary to elicit a response in cytosolic cAMP (Fig. 3C), the stochastic nature of the pulsing may originate from random binding of cAMP to the membrane-bound cAMP receptor. However, the threshold value in the response (0.5 ± 0.1 nM in Fig. 3C; blue curve) is an order of magnitude below the affinity of the receptor (*23*). Because a similar dosage dependence of membrane translocation of a PH domain–containing protein has been observed (*26*), our input/output relation (Fig. 3C, blue curve) most likely reflects the kinetics downstream of the membrane receptors but upstream of PIP_3.

That cells can be oscillatory even at the single-cell level in the perfusion setup (Fig. 3, B, D, and E) might indicate that the emergence of synchronized oscillations in the population is not a collective phenomenon. However, these cell-intrinsic oscillations appear only when the concentrations of extracellular cAMP are kept above 1 nM (Fig. 3B and fig. S9). Before extracellular cAMP can rise to this level spontaneously in a cell population, synchronized pulses must emerge. In our perfusion experiments, at low ρ/k the population remains in a state in which pulses are emitted sporadically. In contrast, when extracellular cAMP is increased to a sufficiently high level, cells become transiently oscillatory. This occurs at high ρ/k where the pulsing frequency reaches a plateau (Fig. 2C). At that level, pulse timing is no longer dictated by the occurrence of random pulses in the population, but rather by an oscillatory mechanism at the single-cell level that gates and paces the timing. As a result, the pulses appear regularly at ~6-min intervals (Fig. 2A). One would expect that disruption of intracellular PDE (RegA) (*27*) should have a strong deleterious effect if these cell-intrinsic oscillatory dynamics involve a feedback regulation via cytosolic cAMP (*20*). However, if the main effect of disrupting RegA is to increase the overall concentration of cAMP secreted into extracellular space, *regA*$^-$ cell populations should still be able to oscillate albeit with only partial synchrony (Fig. 4C) because the extracellular cAMP concentration should almost saturate the dynamic range of the input/output relation (Fig. 3C and fig. S6B). In agreement with this model prediction, we observe that *regA*$^-$ cells oscillate but are poorly synchronized (Fig. 4D). Furthermore, because intrinsic oscillations observed at saturating dose of extracellular cAMP are also present in isolated *regA*$^-$ cells (fig. S10B), the oscillations at the single-cell level do not require a RegA-mediated feedback loop.

Finally, the entire sequence of events in an intact cell population (Fig. 1), from the onset of sporadic firing to determination of the final periodic signaling center, can be inferred from the perfusion experiments. The key enzymes that determine the rates of secretion (r) and of cAMP decay (k) in Eq. 1 are ACA and extracellular PDE, respectively (figs. S1, S2, and S10A), both of which are expressed at very low levels but are induced during the first 4 hours after starvation (*13*, *28*). When cAMP slowly begins to accumulate in the extracellular space, initial pulses are randomly elicited owing to the stochastic subthreshold dynamics at the single-cell level. Although several centers compete for dominance, the results in Figs. 2C and 4B predict that sites that accumulate more extracellular cAMP than others pulse at a higher frequency. Such sites will entrain other sites that fire less often (*10*) and therefore survive. Thus, the first site that accumulates enough extracellular cAMP to support the saturating frequency (~6-min period) becomes the persistent oscillatory center. This not only allows aggregation of more cells to the same location, but may also facilitate later development because cAMP is required for cell differentiation (*29*).

The signaling centers in *D. discoideum* are dynamic entities that self-organize in the population. The onset of synchronized pulses occurs

by a switchlike response of individual cells to an external threshold concentration. The initiation is highly dynamic and collective, because the threshold and the frequency of the response cannot be attributed solely to those at the single-cell level. As random cells continue to emit pulses sporadically, extracellular cAMP accumulates so that, at the peak of the synchronized pulses, cells become transiently oscillatory. The combination of these two strategies, one global and the other local, may allow cells to first determine the global maximum of extracellular cAMP concentration and then aggregate as the pulses become self-sustainable and are periodically emitted from such locations.

References and Notes

1. C. M. Waters, B. L. Bassler, *Annu. Rev. Cell Dev. Biol.* **21**, 319 (2005).
2. A. F. Taylor, M. R. Tinsley, F. Wang, Z. Huang, K. Showalter, *Science* **323**, 614 (2009).
3. S. De Monte, F. d'Ovidio, S. Danø, P. G. Sørensen, *Proc. Natl. Acad. Sci. U.S.A.* **104**, 18377 (2007).
4. T. Danino, O. Mondragón-Palomino, L. Tsimring, J. Hasty, *Nature* **463**, 326 (2010).
5. J. Buck, E. Buck, *Science* **159**, 1319 (1968).
6. S. Yamaguchi *et al.*, *Science* **302**, 1408 (2003).
7. I. H. Riedel-Kruse, C. Müller, A. C. Oates, *Science* **317**, 1911 (2007).
8. K. Wiesenfeld, P. Colet, S. H. Strogatz, *Phys. Rev. Lett.* **76**, 404 (1996).
9. I. Z. Kiss, Y. M. Zhai, J. L. Hudson, *Science* **296**, 1676 (2002).
10. A. T. Winfree, in *The Geometry of Biological Time (Biomathematics Series)* (Springer-Verlag, New York, 1980).
11. D. McMillen, N. Kopell, J. Hasty, J. J. Collins, *Proc. Natl. Acad. Sci. U.S.A.* **99**, 679 (2002).
12. J. Garcia-Ojalvo, M. B. Elowitz, S. H. Strogatz, *Proc. Natl. Acad. Sci. U.S.A.* **101**, 10955 (2004).
13. A. Goldbeter, *Biochemical Oscillations and Cellular Rhythms. The Molecular Bases of Periodic and Chaotic Behaviour* (Cambridge Univ. Press, Cambridge, 1996).
14. K. J. Tomchik, P. N. Devreotes, *Science* **212**, 443 (1981).
15. J. D. Gross, M. J. Peacey, D. J. Trevan, *J. Cell Sci.* **22**, 645 (1976).
16. F. Siegert, C. Weijer, *J. Cell Sci.* **93**, 325 (1989).
17. S. Sawai, P. A. Thomason, E. C. Cox, *Nature* **433**, 323 (2005).
18. G. Gerisch, U. Wick, *Biochem. Biophys. Res. Commun.* **65**, 364 (1975).
19. P. N. Devreotes, P. L. Derstine, T. L. Steck, *J. Cell Biol.* **80**, 291 (1979).
20. M. Maeda *et al.*, *Science* **304**, 875 (2004).
21. V. O. Nikolaev, M. Bünemann, L. Hein, A. Hannawacker, M. J. Lohse, *J. Biol. Chem.* **279**, 37215 (2004).
22. Materials and Methods are available as supporting material on *Science* Online.
23. R. L. Johnson *et al.*, *J. Biol. Chem.* **267**, 4600 (1992).
24. M. C. Dinauer, S. A. MacKay, P. N. Devreotes, *J. Cell Biol.* **86**, 537 (1980).
25. F. I. Comer, C. K. Lippincott, J. J. Masbad, C. A. Parent, *Curr. Biol.* **15**, 134 (2005).
26. L. Bosgraaf, I. Keizer-Gunnink, P. J. Van Haastert, *J. Cell Sci.* **121**, 3589 (2008).
27. P. A. Thomason *et al.*, *EMBO J.* **17**, 2838 (1998).
28. N. Iranfar, D. Fuller, W. F. Loomis, *Eukaryot. Cell* **2**, 664 (2003).
29. L. Kim, A. Harwood, A. R. Kimmel, *Dev. Cell* **3**, 523 (2002).
30. At very low k (flow rates < 1ml/min), the effect of extracellular PDE is nonnegligible. Pulses are no longer observed when dithiothreitol is applied to inhibit extracellular PDE (fig. S2), demonstrating that periodic firing under these conditions depends on degradation of extracellular cAMP by extracellular PDE released by the cells. At higher k, clearing of extracellular cAMP from the medium is mainly determined by dilution.

31. We thank V. O. Nikolaev and M. J. Lohse for providing vector containing Epac1-camps; M. Kitahara and E. Hada for technical help, E. C. Cox, S. Ishihara, K. Kaneko, H. Kori, and J. Teramae for discussions and suggestions; and the Japan Society for the Promotion of Science (JSPS) postdoctoral fellowship (T.G.), K. Kaneko, and the ERATO-JST for support.

Supporting Online Material

www.sciencemag.org/cgi/content/full/science.1183415/DC1
Materials and Methods
Figs. S1 to S10
References
Movie S1

15 October 2009; accepted 19 March 2010
Published online 22 April 2010;
10.1126/science.1183415
Include this information when citing this paper.

Structural Insights into the Assembly and Function of the SAGA Deubiquitinating Module

Nadine L. Samara,[1]* Ajit B. Datta,[1,2]* Christopher E. Berndsen,[1,2] Xiangbin Zhang,[1,2] Tingting Yao,[3] Robert E. Cohen,[3] Cynthia Wolberger[1,2]†

SAGA is a transcriptional coactivator complex that is conserved across eukaryotes and performs multiple functions during transcriptional activation and elongation. One role is deubiquitination of histone H2B, and this activity resides in a distinct subcomplex called the deubiquitinating module (DUBm), which contains the ubiquitin-specific protease Ubp8, bound to Sgf11, Sus1, and Sgf73. The deubiquitinating activity depends on the presence of all four DUBm proteins. We report here the 1.90 angstrom resolution crystal structure of the DUBm bound to ubiquitin aldehyde, as well as the 2.45 angstrom resolution structure of the uncomplexed DUBm. The structure reveals an arrangement of protein domains that gives rise to a highly interconnected complex, which is stabilized by eight structural zinc atoms that are critical for enzymatic activity. The structure suggests a model for how interactions with the other DUBm proteins activate Ubp8 and allows us to speculate about how the DUBm binds to monoubiquitinated histone H2B in nucleosomes.

The covalent modification of chromatin is a core feature of eukaryotic transcription (*1*). The SAGA complex regulates genes transcribed by RNA polymerase II by carrying out multiple functions that include histone acetylation and deubiquitination (*2*, *3*). The 1.8-megadalton SAGA complex, which contains 21 proteins conserved from yeast to humans (*4*), plays a role in transcription activation and also couples transcription elongation with export of the nascent RNA through the nuclear pore complex (*5*). SAGA is recruited to promoter regions by activator proteins, where it catalyzes the cleavage of monoubiquitin from lysine-123 (K123) of histone H2B, as well as acetylation of histone H3 (*6*). Both of these activities are thought to be important for evicting nucleosomes from the promoter region and for facilitating transcription elongation (*7*). The yeast SAGA complex has been a model for studying SAGA function in the transcription cycle. Histone acetylation by SAGA is mediated by the Gcn5 histone acetyltransferase subunit, whereas histone H2B deubiquitination is mediated by a discrete subcomplex known as the deubiquitinating module (DUBm) (*3*, *8*). The yeast DUBm comprises four proteins: the ubiquitin-specific protease (Ubp8) ubiquitin hydrolase, Sgf11, Sus1, and Sgf73 (*9*, *10*). Sgf73 tethers DUBm to the rest of the SAGA complex through a central domain; the N-terminal domain forms an integral part of the DUBm (*9*). Sgf73, along with Sus1, also facilitates SAGA's role in nuclear export by binding to components of the nuclear pore complex (*11*). Although Ubp8 contains a ubiquitin-specific hydrolase (Usp) domain (*12*), the protein is inactive unless it is in complex with the other three DUBm proteins (*9*, *13*). The structural basis for Ubp8 activation is not understood, nor is its dependence on the other three DUBm proteins to form a stable complex that can specifically target H2B for deubiquitination.

Drosophila and human SAGA include a DUBm that functions analogously to the yeast DUBm and comprises homologs of the yeast proteins (*10*, *14*, *15*). In addition, the human DUBm, consisting of USP22, ATXN7L3, ENY2 and ATXN7 (homologs of Ubp8, Sgf11, Sus1, and

[1]Department of Biophysics and Biophysical Chemistry, The Johns Hopkins University School of Medicine, Baltimore, MD 21205, USA. [2]Howard Hughes Medical Institute, The Johns Hopkins University School of Medicine, Baltimore, MD 21205, USA. [3]Department of Biochemistry and Molecular Biology, Colorado State University, Fort Collins, CO 80523, USA.

*These authors contributed equally to this work.
†To whom correspondence should be addressed. E-mail: cwolberg@jhmi.edu